Available online at www.sciencedirect.com
SCIENCE DIRECT
Polymer 47 (2006) 4421–4433
polymer
www.elsevier.com/locate/polymer

Impact fracture behavior of clay–reinforced polypropylene nanocomposites

Q. Yuan [a], R.D.K. Misra [a,b,*]

[a] Center for Structural and Functional Materials, University of Louisiana at Lafayette, P.O. Box 44130, Lafayette, LA 70504-4130, USA
[b] Department of Chemical Engineering, University of Louisiana at Lafayette, P.O. Box 44130, Lafayette, LA 70504-4130, USA

Received 3 March 2006; received in revised form 28 March 2006; accepted 28 March 2006
Available online 27 April 2006

Abstract

The micromechanism of plastic deformation during impact loading of polypropylene–clay nanocomposites is examined and compared with the unreinforced polypropylene under identical conditions of processing to underscore the determining role of clay. The addition of clay to polypropylene increases the impact strength in the temperature range of 0 to +70 °C. Differential scanning calorimetry (DSC), dynamic mechanical analysis (DMA) and transmission electron microscopy (TEM), wide-angle X-ray diffraction (WAXD) and scanning electron microscopy (SEM) techniques provided an understanding of the micromechanism of plastic deformation in terms of the response of the polymer matrix, nucleating capability of the reinforcement, crystal structure, percentage crystallinity, lamellae thickness, and particle–matrix interface. The enhancement of toughness on reinforcement of polypropylene with nanoclay is associated with change in the primary mechanism of plastic deformation from crazing and vein-type in neat polypropylene to microvoid-coalescence-fibrillation process in the nanocomposite.

Keywords: Plastic deformation; Microstructure; Polymer nanocomposites

1. Introduction

Polypropylene (PP) is a semicrystalline thermoplastic polymeric material that has been widely used because of their attractive combination of good processability, mechanical properties, and chemical resistance. However, its inadequate stiffness and brittleness limits its versatile application to some extent. Compounding with inorganic particles is a simple, effective, and economical method to improve the mechanical and thermal properties of PP. A number of studies have been conducted on the structure and property of inorganic particle-filled polymer blends with the objective to identify systems that exhibit superior modulus and yield strength in association with high toughness [1–24].

During the last few years, polymer nanocomposites have attracted significant interest, both in the industry and in the academia. They represent a new class of composite materials containing dispersion of nanometric size (1–100 nm) particles in a polymer matrix that can either be thermoplastic or thermosetting material. Among the different nanoparticles used in polymer nanocomposites, clay is preferred because it provides two distinct opportunities to process polymer clay nanocomposites, viz. intercalation and exfoliation. Experimental investigations indicated that they exhibit a considerable enhancement of strength, modulus, flame-retardant and heat distortion temperature that are not displayed by the individual phases or by conventional composite counterparts [25–28]. In polymer (nylon)–clay nanocomposite, the clay particles are about the same size as the polymer molecules themselves, which enables them to be intimately mixed and chemically bonded to each other [29]. It is presently believed that the local and global conformation of the polymers within the host galleries of nanoparticles are dramatically different from those observed in the bulk because of the confinement of the polymer chain and also due to specific polymer–surface interaction normally not observed in the bulk [13]. It is also believed that the local and chain dynamics are greatly affected by the confinement as well as the polymer–surface interactions. The basic reason for the synergistic improvement in properties is far from understood and the current thinking is that nanoparticle effects are related to optically confined polymer matrices, quantum size effects, and columbic-charging effects originating from ultra fine sizes, morphology, and interfacial interactions of the phases involved [30–32].

* Corresponding author. Address: Center for Structural and Functional Materials, University of Louisiana at Lafayette, P.O. Box 44130, Lafayette, LA 70504-4130, USA. Tel.: +1 337 482 6430; fax: +1 337 482 1220.
E-mail address: dmisra@louisiana.edu (R.D.K. Misra).

0032-3861/$ - see front matter © 2006 Elsevier Ltd. All rights reserved.
doi:10.1016/j.polymer.2006.03.105

The significant increase of clay-reinforced nanocomposites in modulus is recognized and is reasonably understood. However, an understanding of the toughness behavior is still fragmented and less examined. It is important to examine impact toughness considering that the majority of semi-crystalline polymeric materials (polyethylene and polypropylene) are ductile at low strain rates, but at high strain rates such as those experienced in Izod impact test, exhibit a brittle behavior. Thus, the study of impact toughness at high strain rates is of particular interest and relevance because yield stress increases with strain rate, promoting brittle mode of fracture. Lastly, high tensile toughness may not necessarily mean high impact toughness.

The toughening behavior in polyvinylidene fluoride (PVDF) [33] and glassy polymer polylactide-*co*-glycolide (PLG) [34] by layered silicates nanoparticles (nanoclay) was recently examined by Giannelis et al. via tensile tests. The significant enhancement in tensile elongation on reinforcement of PVDF with nanoclay was attributed to the reduction in spherulite size and the formation of the more mobile β-fiber-like crystallites. In the case of PLG–clay nanocomposites, crazing and shear yielding that require adequate mobility of polymer chain segments for plastic flow process contributed to greater percentage elongation-to-fracture of the nanocomposite. It was proposed that the polymer chains in the crazed zone were easily pulled into the fibrils of the craze, leading to extensive stretching of the fibrils. In contrast to the clay reinforced nanocomposites, the enhancement of impact strength of calcium carbonate reinforced high density PE composites, where the rigid particles in comparison to clay are non-layered and nearly spherical was attributed by Tanniru and Misra [23] to the particle-induced cavitation and fibrillation. This process was encouraged by the amorphous nature of the particle–matrix interface. In comparison to crazing-tearing, the particle-induced cavitation process released plastic constraint and encouraged plastic deformation of the matrix [23].

The effect of matrix (homopolymer or heterophasic copolymer) on the mechanical properties of PP–clay nanocomposites was also investigated by the Gianellis group [35]. Our recent studies on polyethylene (PE)–clay nanocomposites [36] indicated that the addition of clay to PE decreased the impact strength in the test temperature range of −40 to +70 °C, but the toughness continued to be the high at ∼10 kJ/m^2, even at low testing temperature (−40 °C). In the present paper, we describe the impact toughness behavior of polypropylene (PP)–clay nanocomposites in terms of the response of the polymer matrix, in terms of nucleating capability of the reinforcement filler, crystal structure, percentage crystallinity, lamellae thickness, and matrix–particle interface, using identical clay and procedure reported for polyethylene (PE)–clay nanocomposite system. It is intriguing to note that in contrast to polyethylene (PE)–clay nanocomposite system, the polypropylene (PP)–clay system is characterized by enhancement in toughness. Possible reasons for the differences in impact toughness behavior are discussed.

2. Experimental procedure

2.1. Materials

A commercially available grade of polypropylene (PP) produced by Basell Polyolefins (product name: Profax 632) was used to process PP-4 wt% clay and PP-8 wt% clay nanocomposites. This grade of PP has a melt flow rate of 12 g/10 min at 230 °C/2.16 kg. A natural montmorillonite clay surface-modified with dimethyl dialkyl ammonium (Nanomer I.44P, Nanocor) was used as the reinforcement filler. The nanocomposites were prepared by mixing the appropriate amounts in a twin screw extruder (counter rotating, 100 rpm) followed by injection molding of tensile and Izod impact bars.

2.2. Crystallization behavior, structural characteristics, and dispersibility

The change in percentage crystallinity, and structural characteristics induced by clay is important in understanding the deformation behavior along with its dispersion. The crystallization behavior of neat PP and clay-reinforced PP nanocomposites was studied by differential scanning calorimetry (DSC) (TMA, DSC 2910) in a flowing nitrogen atmosphere. The neat PP and PP–clay nanocomposites were heated from 30 to 200 °C and held at the high temperature for about 3 min in order to erase the previous thermomechanical history and to obtain a completely relaxed melt. Then the melt was cooled to 30 °C at the rate of 10 °C/min, and a second scan was carried out at the rate of 10 °C/min.

The dispersibility and intercalation of PP into the clay layers was studied by transmission electron microscopy (TEM). The staining was carried out in the vapor phase. The trimmed specimen was stained by staining with solid ruthenium tetroxide (RuO_4) for 10 h in a vial. Sections of ∼100–200 nm were cut using a Leica ultramicrotome equipped with a diamond knife and collected in a trough filled with water and placed directly on 400-mesh copper grids. Transmission electron micrographs were taken with Hitachi H-7600 at an acceleration voltage of 100 kV.

2.3. Mechanical properties

The tensile bars of neat PP and PP–clay nanocomposites were tested in uniaxial tension at 20 °C using a computerized MTS 210 tensile testing machine at selected displacement rate of ∼5 mm/min to determine tensile properties (modulus, yield strength) in accordance with ASTM D-638. The Izod impact tests were carried out using an instrumented falling weight Tinius Olsen impact tester (Model 899) with an impact velocity of 1 m/s. The notched specimens were subjected to the impact test in the temperature range of −40 to +70 °C. The storage modulus of neat PP and PP–clay nanocomposites was studied by dynamic mechanical analysis (DMA). This process was carried out using a TA Instruments 2980 in a single cantilever mode from −120 to 130 °C. The testing frequency was 1 Hz and the heating rate was 3 °C/min.

2.4. Wide-angle X-ray diffraction (WAXD)

The wide-angle X-ray diffraction patterns were analyzed on a Scintag, XDS 2000 X-ray diffractometer, operating at 43 kV and 21 mA using Cu Kα radiation of wavelength 1.54 Å as the X-ray source. Samples were scanned at a rate of 1.0°/min in the 2θ range of 3–40°.

2.5. Morphological characterization

The fracture surface of Izod impact tested specimens at −40 °C was studied using field emission SEM (JEOL 6300F) after coating with gold to minimize electrostatic charging. The fracture surface morphology of neat PP and PP–clay nanocomposites was observed using SEM. In order to characterize the effect of nanoclay particles on the nature and size of spherulite of PP, a Linkam CSS-450 high temperature stage (Linkam Scientific Instruments Ltd, Tadworth, Surrey, UK), equipped with polarizing light microscope (Olympus BX45) was used. The gap between the windows was set as 20 μm. The samples were isothermally crystallized at 150 °C after removing thermal history at 200 °C for 5 min and the micrographs were taken in situ by Olympus digital microscope camera (type DP12).

3. Results and discussion

3.1. Tensile properties

The tensile properties of neat PP and PP-4 wt% clay nanocomposite are listed in Table 1. The elastic modulus increased from 0.54 GPa in neat PP to 0.83 GPa in 4 wt% clay nanocomposite. Also, with the addition of nanoclay, the yield stress increased from 33 to 38 MPa. The increase in yield stress was consistently observed on repeated tests. The increase of modulus and yield stress are attributable to the reinforcement effect. A similar behavior has been recently observed for other clay-reinforced nanocomposite systems [24,37]. To further understand this behavior, DSC, DMA, TEM and polarizing light microscope (PLM) were employed to investigate the crystallization behavior, crystal structure and particle-matrix interface.

Table 1
Physical and mechanical properties of neat PP and PP-4 wt% clay nanocomposites

Material	Neat-PP	PP-4 wt% clay
Heat of fusion (J/g)[a]	95	97
%Crystallinity (DSC)[a]	45	46
Crystallization temperature (°C)	114	127
Melting temperature (°C)	164	166
Lamellar thickness (nm)	5.32	5.82
Average spherulite size (μm)	210	14
Storage modulus at 25 °C (GPa)	2.2	3.3
T_g (°C)	9.2	10.0
Young's modulus (GPa)	0.54	0.83
Yield stress (MPa)[b]	33	38

[a] For 100% polymer.
[b] Engineering stress related to initial sample cross-section.

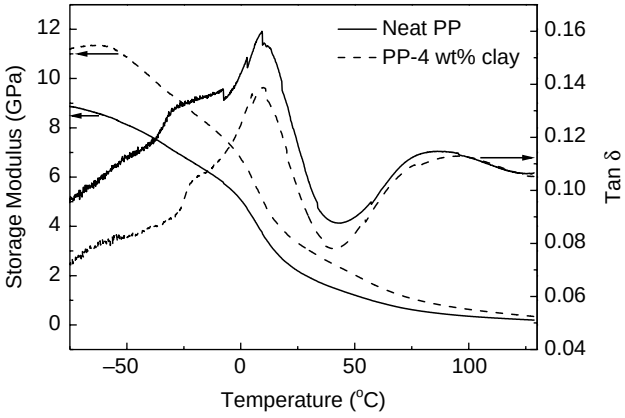

Fig. 1. Dynamic mechanical analysis (DMA) plot of neat PP and PP–clay nanocomposite.

3.2. Dynamic mechanical analysis (DMA)

The spectra of dynamic mechanical analysis for neat PP and PP-4 wt% clay nanocomposite are presented in Fig. 1. The DMA measurements indicate that stiffness is significantly increased over the entire investigated temperature range on incorporation with clay (Table 1).

3.3. Crystallization and Structural characteristics

Crystallization behavior of neat PP and PP–clay nanocomposites (melting and crystallization temperature, heat of fusion and crystallinity) obtained from DSC experiments (Fig. 2) is summarized in Table 1. Table 1 shows that the melting and crystallization temperatures of PP are significantly increased with the addition of clay. The crystallization temperature (T_c) is increased by ~13 °C, when the content of clay increased to 4 wt%. This is ascribed to the nucleating effect of nanoclay. However, the heat of fusion and crystallinity of PP appeared to

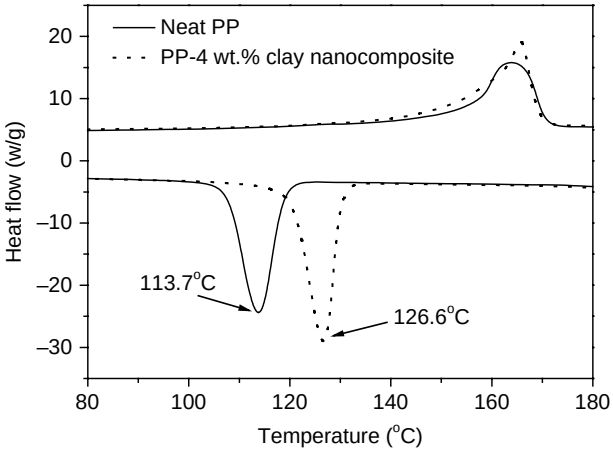

Fig. 2. Differential scanning calorimetry plots for neat PP and 4 wt% clay–reinforced PP nanocomposite.

be unaffected on reinforcement with clay. The crystallinity of PP was estimated using a heat of fusion of 209 J/g for 100% crystalline PP [38]. Also, listed in Table 1 is lamellar thickness (l) estimated using the Thomson–Gibbs equation [39]:

$$l = \frac{2\gamma T_m^0}{\Delta H_0 \rho (T_m^0 - T_m)} \quad (1)$$

where T_m^0 is the equilibrium melting temperature, T_m is the detected melting temperature by DSC, γ the surface free energy, ΔH_0 the heat of fusion for 100% crystalline PP, and ρ the density. The melting temperature (T_m) and lamellae thickness followed a similar trend, i.e. greater lamellae thickness of the nanocomposite was characterized by higher melting temperature, as expected (Table 1).

In Fig. 3, polarized light micrographs of the 150 °C crystallized neat PP and PP–clay nanocomposites are presented and the size of the spherulite size derived from Fig. 3 is listed in Table 1. It may be noted from Table 1 that the average size of the spherulite is dramatically reduced from ~210 to 14 μm on reinforcement with clay. This reduction in size is ascribed to the nucleating effect of clay. The decrease in spherulite size is caused by higher nucleation density induced by the clay. It was observed that at a relatively lower crystallization temperature of 142 °C, asymmetric fibrous crystals formed in the clay nanocomposite [40]. However, in our case, petal-like crystals form in PP–clay nanocomposite. These observations lead us to suggest that the addition of clay is not necessary to obtain fibrous crystals, which were previously ascribed to the crystallization of oriented iPP chains induced by shearing [41,42].

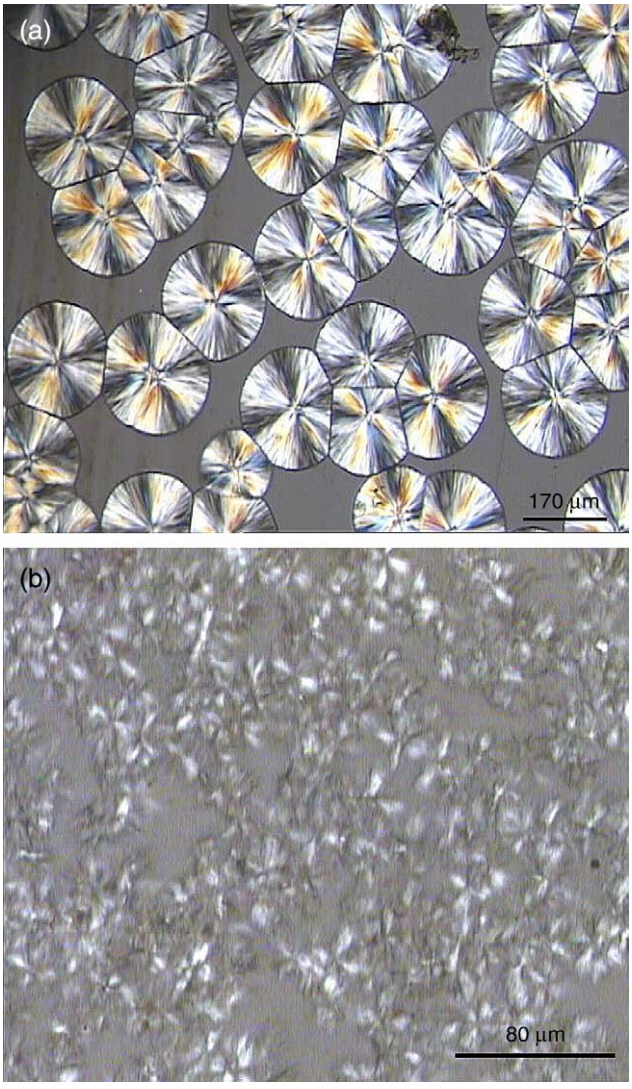

Fig. 3. Polarizing light micrographs of neat PP and 4 wt% clay–reinforced PP nanocomposite crystallized at 150 °C. (a) Neat PP and (b) 4 wt% clay reinforced PP nanocomposite.

3.4. Dispersion and intercalation of clay

Transmission electron micrographs of microtomed section (~100 nm) of PP-4 wt% clay nanocomposite confirming uniform distribution and intercalated structure is presented in Fig. 4a and b. Uniform dispersion is important because if the matrix consists of aggregates of particles, the stress field in the vicinity of the aggregate will be high, resulting in easier crack initiation and propagation, and consequent premature failure. The higher magnification TEM micrographs (Fig. 4b–d) describe intercalation of clay. We can say from Fig. 4b–d that crystalline lamellae are parallel to the clay platelets and are present between the intercalated galleries of clay (Fig. 4c and d). Similar observations were recently made by us in the PE–clay nanocomposite system [43]. We believe that the interphase around clay is characteristic of a crystalline nature based on the existence of parallel lamellae in the vicinity of the clay.

Based on the above results, the increase in tensile modulus and yield stress in PP–clay nanocomposite can be attributed to the reinforcement of clay. Generally, an increase in crystallinity or increase in spherulite size increases the modulus because large spherulites are envisaged to exhibit appreciably higher load bearing ability. In the present study, upon the reinforcement of PP with clay does not appear to significantly influence crystallinity. However, the spherulite size was significantly decreased. The reinforcement has a positive effect on modulus and yield strength, while the nucleating effect of clay has a negative effect. The reinforcement effect overrides any influence of the small spherulite size. However, the mechanical behavior of the nanocomposites is not straightforward and is not a simple function of spherulite size and crystallinity, but is a complex function of other factors including lamellae thickness and nature of the interface. Table 1 shows that lamellae thickness was marginally increased on reinforcement with nanoparticle of clay. The lamellae thickness is an important controlling parameter in the activation of yield, and yield strength in semi-crystalline polymers is directly proportional to lamellae thickness [44]. The above observations suggest that it is the reinforcement effect that increases modulus and yield strength.

3.5. Izod impact toughness

Fig. 5 shows the notched Izod impact strength of PP and PP-4 wt% clay nanocomposite obtained in the temperature range

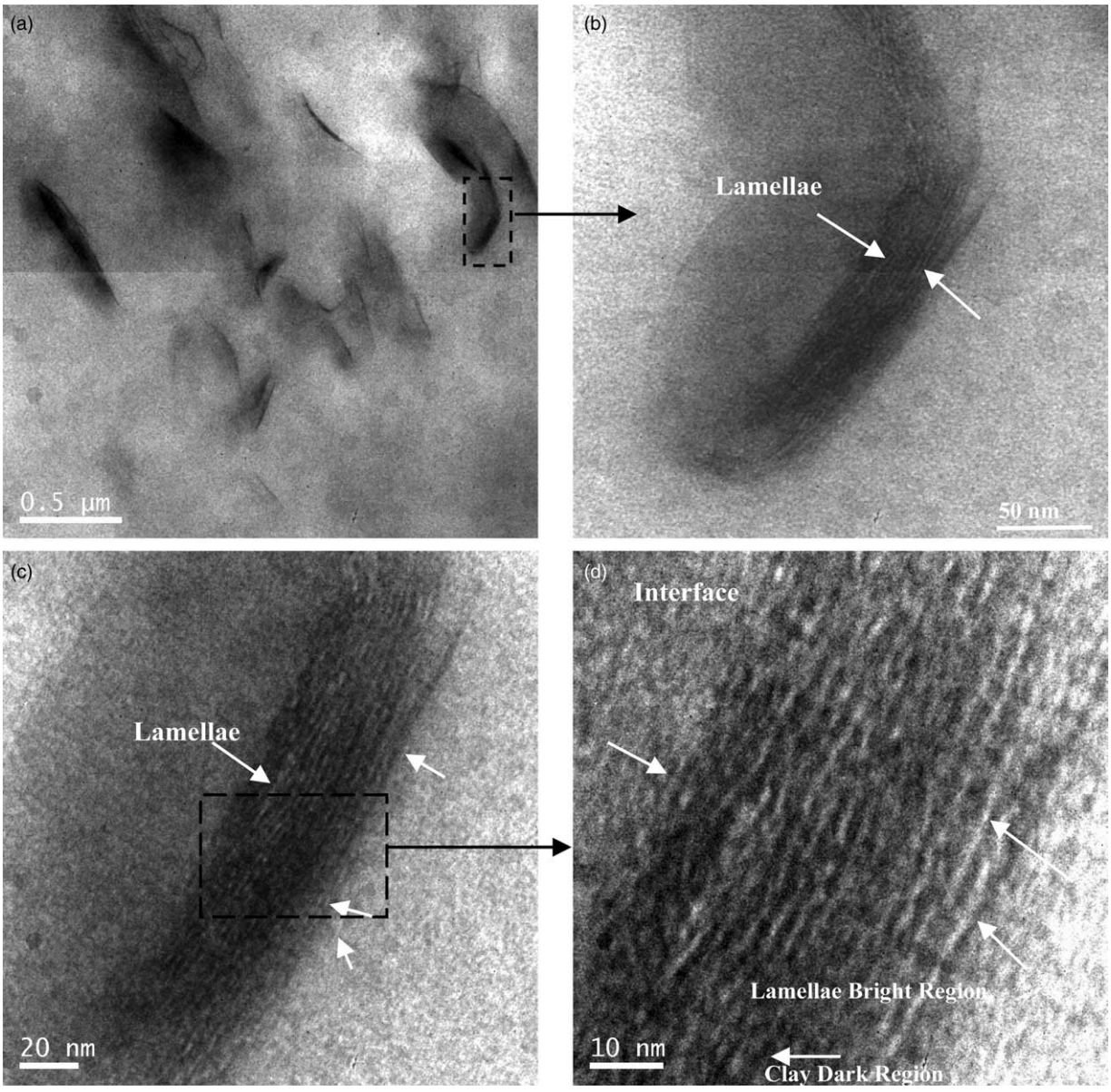

Fig. 4. Transmission electron micrographs of PP-4 wt% clay nanocomposites showing uniform distribution of clay and the interface between PP and clay. Black regions are clay and white regions are crystalline lamellae.

of −40 to +70 °C. It may be noted that the addition of clay to PP significantly increases the impact strength in the temperature range of 0 to +70 °C, while the toughness remains unaffected below 0 °C.

3.6. Fractography

In general, the fracture characteristics of neat PP (also PP–clay nanocomposite) were similar at the investigated temperature of −40 to +70 °C, except that the regions of sub-zones moved away from the notch side at higher test temperatures. Thus, the SEM micrographs are presented for representative temperature of 20 °C. Representative SEM micrographs of the fracture morphology of neat PP and 4 wt% clay reinforced PP are presented in Figs. 6, 7, and 9–11. We first describe the fracture characteristics of neat PP.

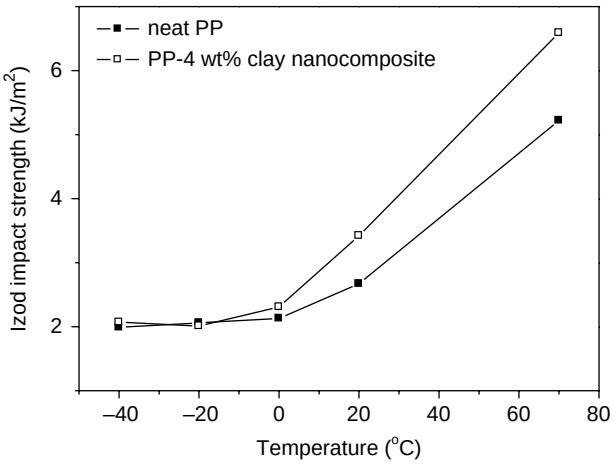

Fig. 5. Izod impact strength for neat PP and 4 wt% clay–reinforced PP nanocomposite as a function of temperature.

3.6.1. Fracture characteristics of neat polypropylene

Fig. 6 presents the fracture surface of neat PP impact tested at 20 °C. Apparently, the fracture surface contains different distinct zones. From Fig. 6, two primary zones can be defined and include initiation zone (zone 1) and the crack propagation zone (zone 2) (Fig. 6a); the crack propagates from left to right. Zone 1 (fracture initiation zone) is a small zone compared to zone 2 (crack propagation zone). The fracture initiation zone 1 has a craze-like brittle appearance. Compared to PE [43], zone 1 shows less ductile or brittle-like behavior, consistent with the lower value of Izod impact strength for PP in relation to PE. The breakdown of the craze initiation zone leads to the crack propagation region (zone 2). Zone 2 is a zone associated with crack propagation, and can be further classified into five zones:

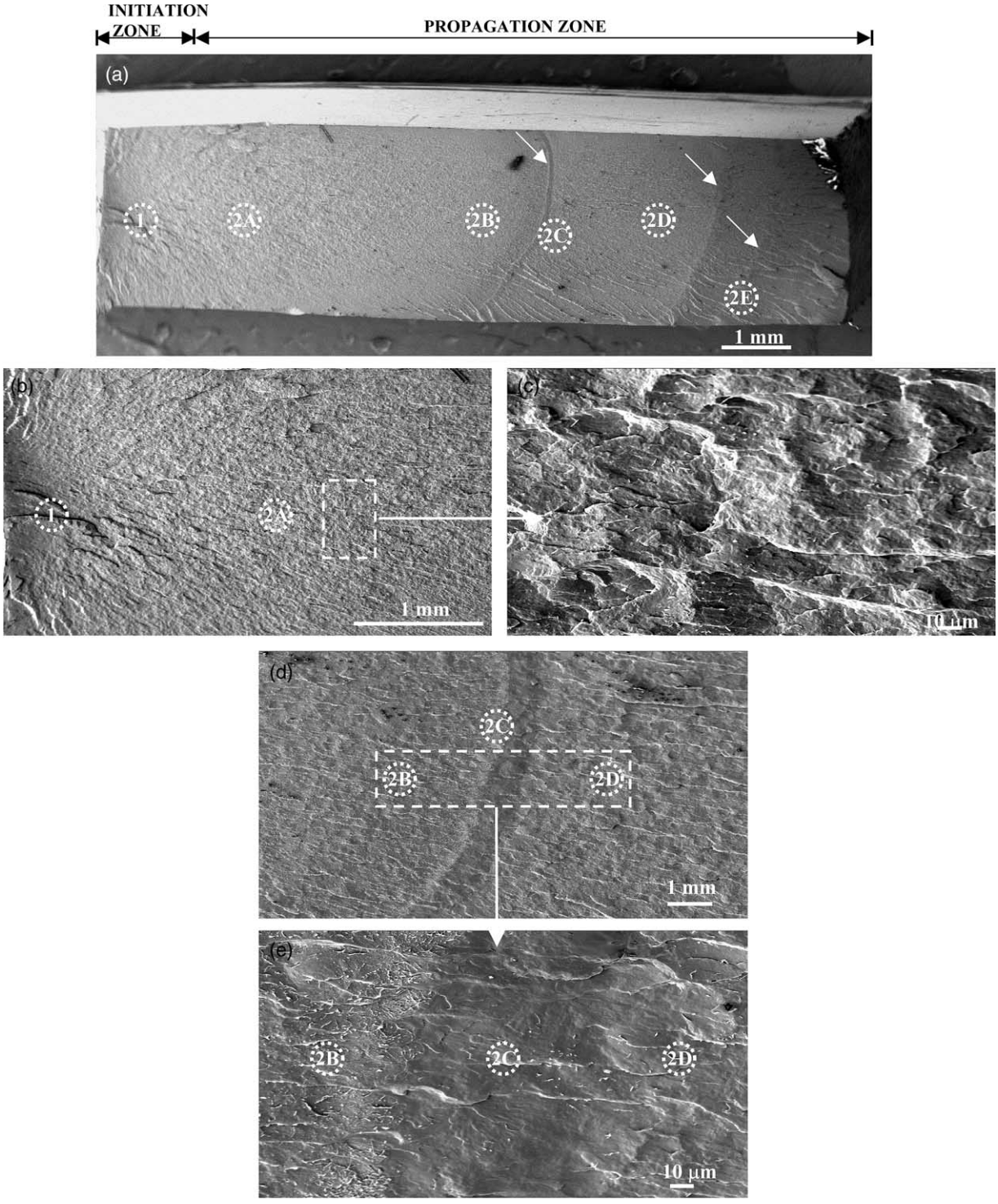

Fig. 6. Scanning electron micrographs of the fracture surface of neat PP impacted tested at 20 °C showing initiation (zone 1: craze-like zone) and different propagation zones (zone 2A: brittle-like; zone 2B: less brittle-like zone with small vein-type features; zone 2C: stick-slip; zone 2D: slow shear zone and zone 2E: rapid shear zone) at different magnifications.

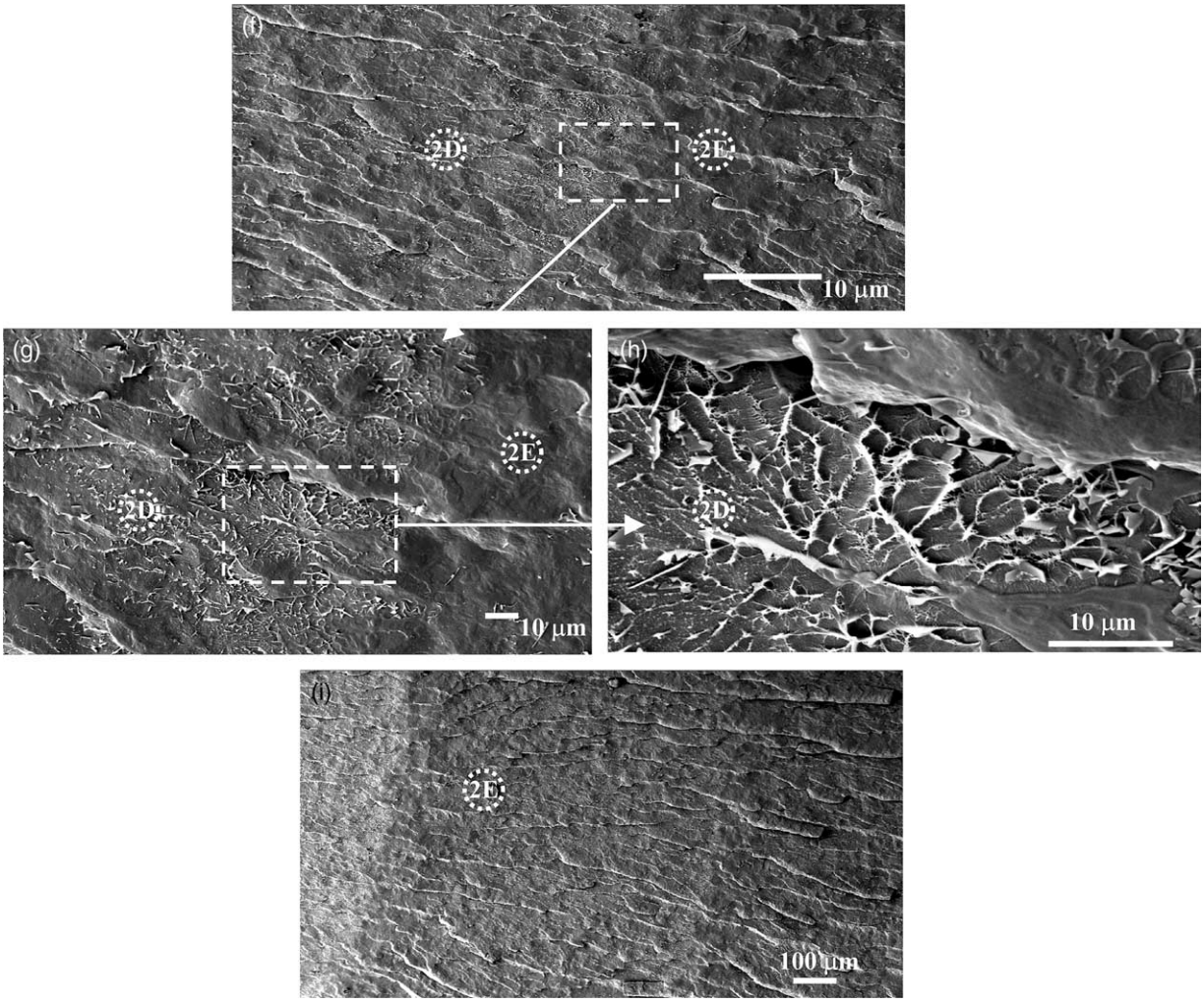

Fig. 6 (*continued*)

(a) brittle-like zone (2A), (b) less brittle-like zone with small vein-type features (2B), (c) prominent stick-slip zone (2C), slow shear zone (2D), and rapid shear zone (2E). Stick-slip process was also observed at later stages of crack propagation and is indicated with arrows in Fig. 6a. Zone 2A is the extended region of fracture initiation, characteristic of rapid crack growth and brittle appearance (Fig. 6b). The brittle characteristic is evident in the higher magnification micrograph (Fig. 6c). The occurrence of zone 2A can be visualized as sudden burst of energy on the breakdown of the craze zone. The crack propagates at a rate, which is of high magnitude such that the material does not have adequate time to respond, leading to brittle fracture zone 2A ahead of the initiation zone (i.e. 2A: commencement of propagation zone). However, as crack propagation proceeds, the rate of crack propagation slows down with consequent decrease in brittle appearance and existence of feeble river-like or chevron markings (zone 2B, Fig. 6d and e). The chevron-type markings are produced by shallow ridges and valleys on the surface. The crack front is well defined implying some irreversible deformation must have occurred at the crack tip leaving these residual markings on the fracture surface.

An interesting characteristic feature of the fracture surface of neat PP is a small zone (2C) that occurs as a parabolic ridge or a thin curved band with a defined boundary on the macroscopic fracture surface. This feature resembles the stick-slip type propagation observed during the scratch deformation in polymeric materials [45]. It represents stop-go crack front, as evident in the high magnification micrographs of zone 2C (Fig. 6e). It is expected that the stop-go-process is accompanied by stress relaxation. Subsequently, reinitiation of crack occurs along this crack front such that crack growth is accompanied by a series of fine river line steps that can be seen in the vicinity of stop-go boundary in the low magnification Fig. 6a. With progress in stick-slip or stop-go propagation, a new crack zone (zone 2D) is initiated that grows unstably until the strain energy release rate is sufficient for further crack growth. This can be seen further in the fracture surface morphology in zone 2D. If this was not the case, then the features of fracture surface should have been similar in zones 2C and 2D. Zone 2D at high magnification (Fig. 6f–h) shows vein-type pattern. Similar vein-type pattern results when two glass slides, separated by a film of oil are pulled apart. During this process, cavities form in the oil and they expand by

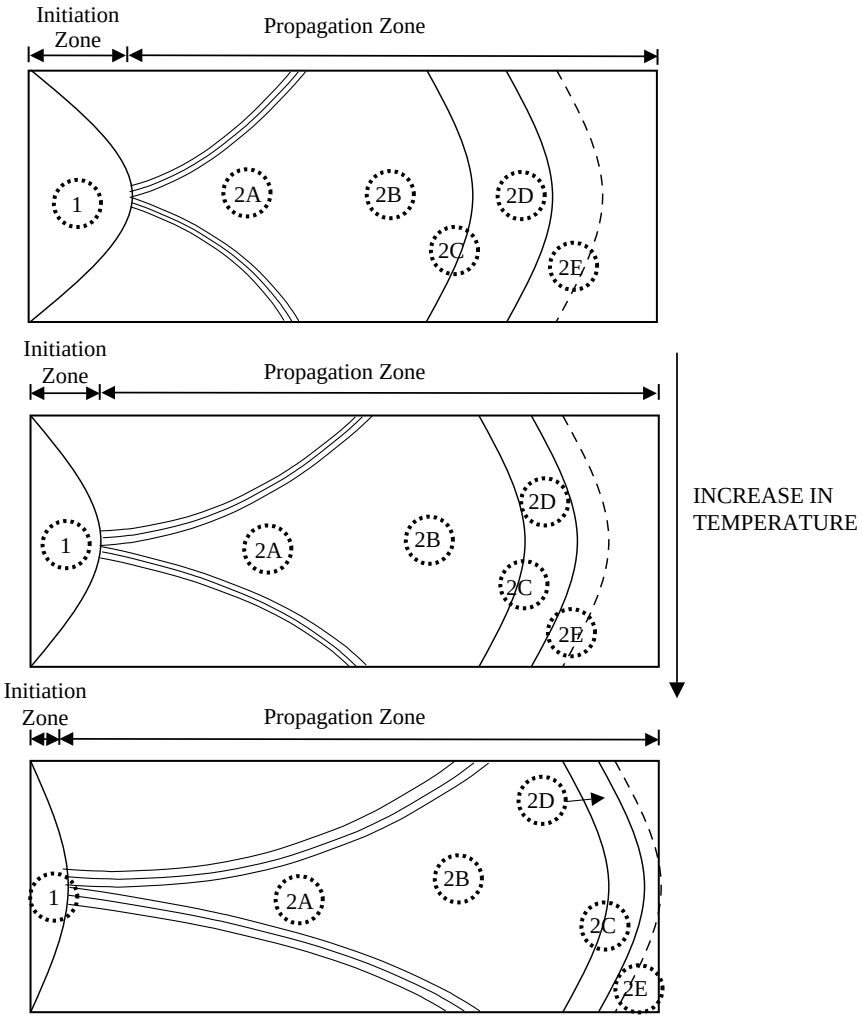

Fig. 7. Schematic of the extent of initiation and propagation zones as a function of temperature in neat PP.

fingering growth. Such an observation suggests that it is highly sheared region involving tearing of presumably amorphous part of PP. It may also be noted that the vein-type morphology in zone 2D has some similarity to the end region of zone 2B (i.e. before the stop-go process) (Fig. 6e), if we were to compare the high magnification micrograph of zone 2D (Fig. 6g) with zone 2B (Fig. 6e).

Ahead of zone 2D, two more stop-go crack fronts were observed and are identified by arrows in Fig. 6a. These stop-go crack fronts are analogous to the periodic parabolic cracks observed during scratch deformation of polymeric materials [45]. Stick-slip or stop go propagation, associated with the dynamic crack propagation effects, occur when the speed of the crack is below the critical value—the crack stops or arrests (sticks). When the stress increases or builds-up again, the crack re-initiates and propagates (slips). During the stick-slip stage, local deformation occurs around the stopped crack involving some stable growth.

The zone 2E is a rapid crack-growth zone with terraced or chevron features that terminate when fracture occurs. This feature microscopically dominated in zones 2B, 2D, and 2E suggesting that the primary mechanism of deformation is similar in three zones even though the zones are preceded by the stop-go process.

Also, with increase in test temperature, the stop-go crack front zone moved further away from the root of the notch, as schematically shown in Fig. 7. This is because the stop-go process depends on the test conditions. At low temperatures, there is rapid acceleration of crack growth such that the critical stress necessary to propagate is quickly reduced, whereas at higher temperatures it decreases at a later stage of crack propagation. Also, at a later stage, it is expected that the crack blunting during the ‘stick’ stage will be reduced. The extent of the craze-like zone (zone 1) was also reduced with increase in test temperature.

3.6.2. Fracture characteristics of clay–reinforced polypropylene

In contrast to neat PP, the overall macroscopic fracture surface behavior of PP–clay nanocomposite at 20 °C appears relatively more ductile-like (Fig. 8), and relatively rougher than neat PP (Fig. 6). In a manner similar to neat PP, we can define two primary zones: initiation zone (zone 1) and propagation zones (zone 2). However, the nature of fracture surface

morphology in these two zones was different from neat PP. Generally, the characteristics of the fracture surface were similar at all the test temperature except for the extent of the individual zones. Fig. 8 presents the macroscopic and microscopic features of 20 °C impact loading fracture surface of PP-4 wt% clay nanocomposite.

A primary difference in the macroscopic fracture surface of clay reinforced PP from the fracture surface of the un-reinforced PP was that the stop-go process zones moved further away from the notch, as schematically shown in Fig. 9. The second macroscopic difference was that the parabolic or curved boundaries associated with the stop-go process were not very distinct.

In a manner similar to neat PP, the crack initiation zone (zone 1) was characterized by a craze-like zone, which was smaller in size compared to neat PP under identical test condition (see schematic Figs. 7 and 9). Also, the flow lines commencing at the end of the craze zone 1 extended further inside the specimen, consistent with the increase of plastic flow of material (high impact strength) in clay reinforced PP (Figs. 6a and 8c and schematic Figs. 7 and 9). The propagation zone can be classified into three distinct sub-zones as shown in Fig. 8a: (a) brittle-like zone (2A), (b) stick-slip zone (2B) and (c) stick-slip and shear lip zone (2C). In neat PP, the rapid breakdown of the craze initiation zone does not provide adequate time for the material ahead of the initiation zone to respond, resulting in brittle-like fracture surface. However, the high toughness of the nanocomposite results in slower breakdown of the initiation zone and is characterized by an initial propagation zone (2A), which has a macroscopically

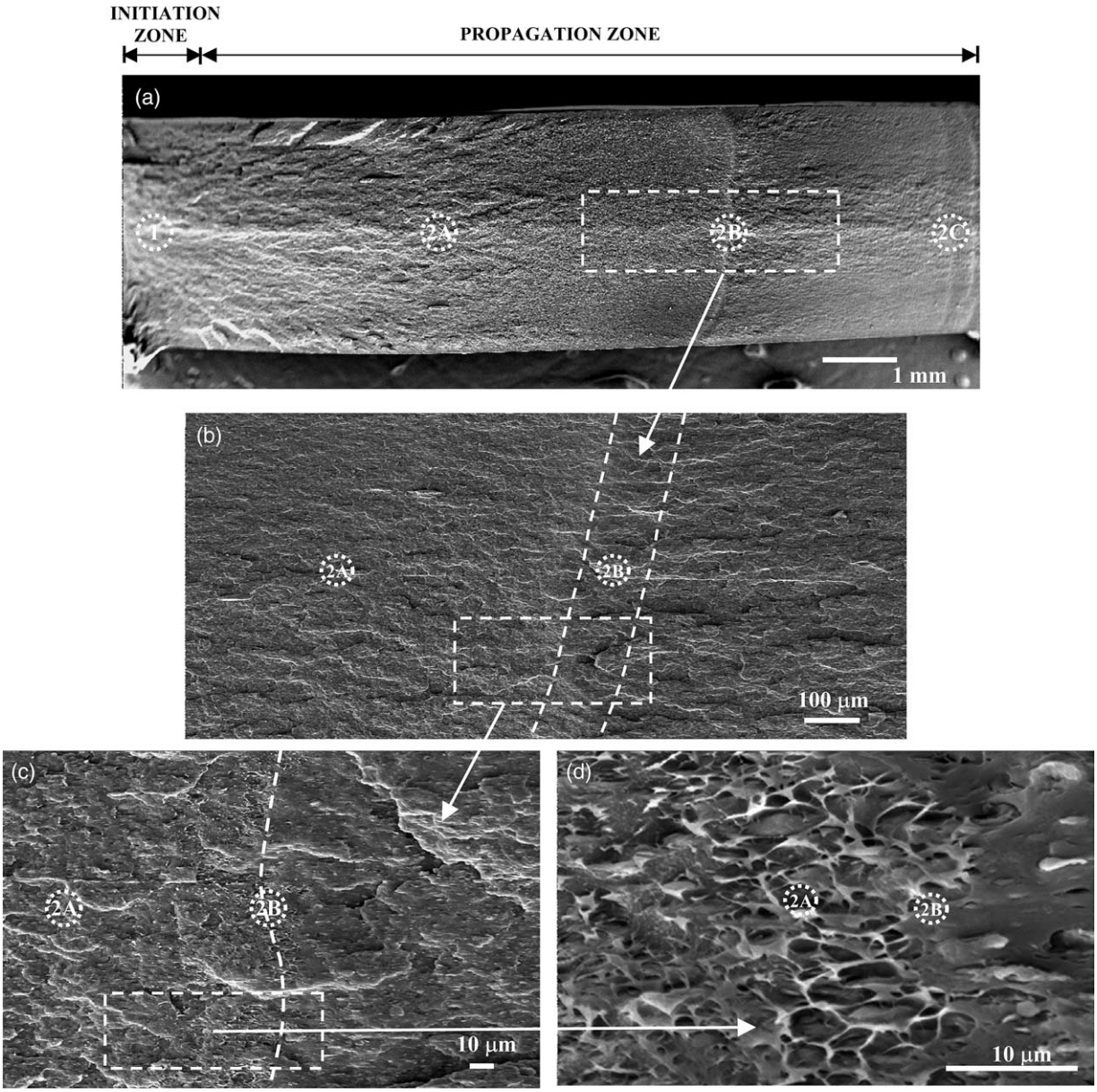

Fig. 8. Scanning electron micrographs of the fracture surface of PP-4 wt% clay nanocomposite impacted tested at 20 °C showing initiation (zone 1) and propagation zone (zone 2). Similar behavior was observed at other temperatures.

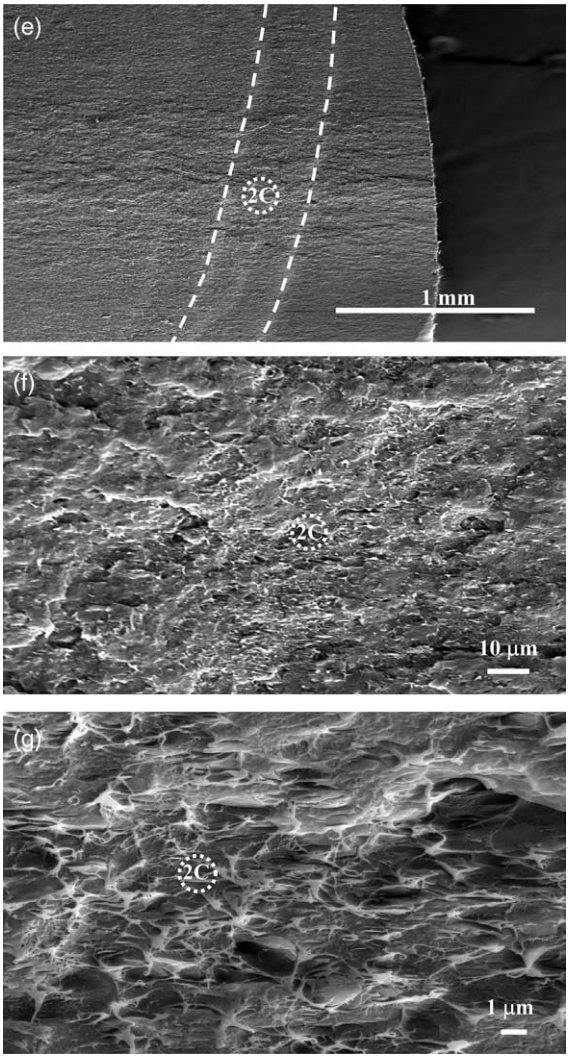

Fig. 8 (*continued*)

rougher surface (zone 2A in Fig. 8a) than neat PP. At high magnification, this zone is characterized by a combination of microvoids of size 2–5 μm together with some deformation of ligaments between the microvoids. The second propagation zone (zone 2B) was a stick-slip zone characterized by the parabolic ridges. In a manner similar to neat PP, three crack-arrest fronts were observed. However, as stated above, they occurred at a distance further away from the notch such that second and third one was close to each other and occurred during the last stage of fracture. As discussed above, this observation again implies that the crack propagation proceeds slowly in the nanocomposite. Thus, the envisaged stop-go parabolic ridges reflect the resistance to crack growth and the crack must have been temporarily slowed at these parabolic ridges [46]. Moreover, the formation of stick-slip zone has been shown to be related to the blend morphology [47]. High percentage of fibers and thicker fibers resulted in larger ridges. Our results indicate that the higher toughness reduces the distance between the two adjacent parabolic ridges.

The surrounding of the last propagation zone is a shear-lip zone (zone 2C) (Fig. 8a and b) and is similar to zone 2A, characterized by a combination of large and small size microvoids and fibrillation. During the impact tests, the elements of the material (largely amorphous content) or ligaments between the microvoids draw down to fine points, before separation of polymer molecules past each other occurs, producing fibrillated fracture. The highly stretched material then shrinks producing an appearance presented in the high magnification micrograph of zone 2C in Fig. 8c. The combination of microvoid and fibrillated fracture can be understood in terms of two interactive processes. First, the nucleation of microvoids in the vicinity of particles provides stress concentration centers that determine the density of microvoids. Second, the viscoelastic plastic processes associated with the growth of microvoids and the deformation of ligaments bridging the microvoids. The ligaments or islands of material between the microvoids must fracture before the final separation occurs. An explanation for the mechanics of fracture necessitates a model that can predict the nucleation, density, and growth of microvoids, all of which dependent on the state of stress. We are currently examining this aspect. A schematic of the envisaged microvoid coalescence-fibrillated fracture process is presented in Fig. 10. A schematic of the relative extent of different zones is summarized in Fig. 9. The initiation zone (zone 1) was observed to decrease with increase in temperature with consequent increase in the zone 2A, which was ductile in nature. In summary, comparing with neat PP, the fracture surface of clay–reinforced PP was ductile in nature and this is consistent with the result of Izod impact test (Section 3.5).

3.6.3. Toughness of clay–reinforced polypropylene nanocomposites

It is clear from the relative comparison of the initiation and propagation zone in neat PP and PP-4 wt% clay nanocomposite that the reinforcement leads to transformation of the fracture surface from predominantly craze-like and vein-type features (Fig. 6b) to predominantly a combination of microvoid coalescence and fibrillation fracture (Fig. 8b). On comparing with the fracture behavior of neat PP and PP-4 wt% clay nanocomposite, we believe that nanoclay must be the source of microvoid nucleation [43]. The matrix ligaments between these voids are extensively deformed in the propagation zone, particularly in the later stage (zone 2C and surrounding) leading to a combination of microvoid coalescence and fibrillated fracture.

The toughness of a material is generally related to the energy dissipating events that occur in the vicinity of a sharp crack. In the nanocomposite, the microvoids are responsible for high toughness. These microvoids release the plastic constraint in the matrix, triggering large-scale plastic deformation with consequent tearing of matrix ligaments between microvoids. While in the neat PP, only crazing contributes to energy absorption, in general, this could not absorb too much energy resulting in brittle fracture behavior. Thus, there is a clear relationship between the fracture mode and impact strength of neat PP and clay reinforced nanocomposites. Previous work on neat polymers indicated that higher crystallinity and large

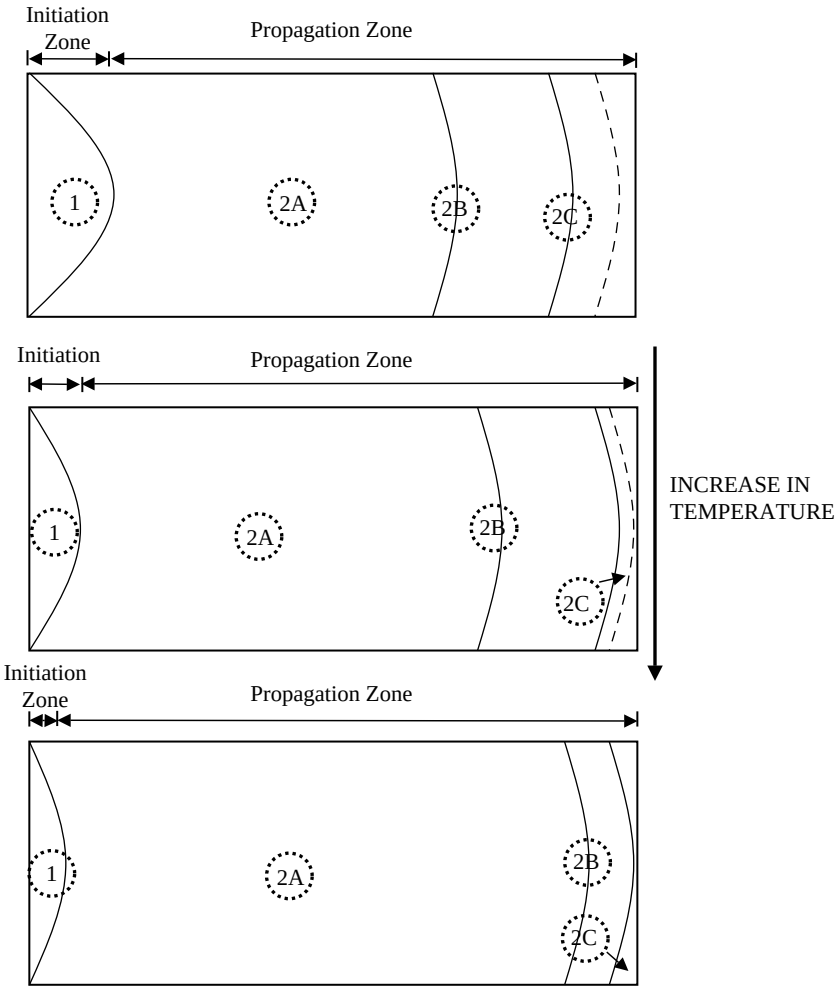

Fig. 9. Schematic of the extent of initiation and propagation zones as a function of temperature in PP–clay nanocomposite.

spherulite size are detrimental to toughness [22]. As described in Section 3.3, the reinforcement with clay did not increase percentage crystallinity, but slightly increased lamellae thickness and significantly decreased the spherulite size (Table 1). The observation of decrease of spherulite size in the nanocomposite is expected to have a positive effect on toughness.

Moreover, it is known that the nanoclay particles have both nucleation and suppression effects on the crystallization of polymer matrix and this is related to the dispersion state of clay [48,49]. From the electron microscopy and X-ray diffraction studies, we believe that the reason for the weaker nucleating effect of clay in PE [43] as compared to the present study on PP is most likely to be related to the different dispersion state of clay in the two matrices, the nanoclay particles in PP–clay nanocomposite disperse better than in clay–reinforced PE nanocomposite and this is supported from the WAXD results. The clay and the processing procedure were same in our recent

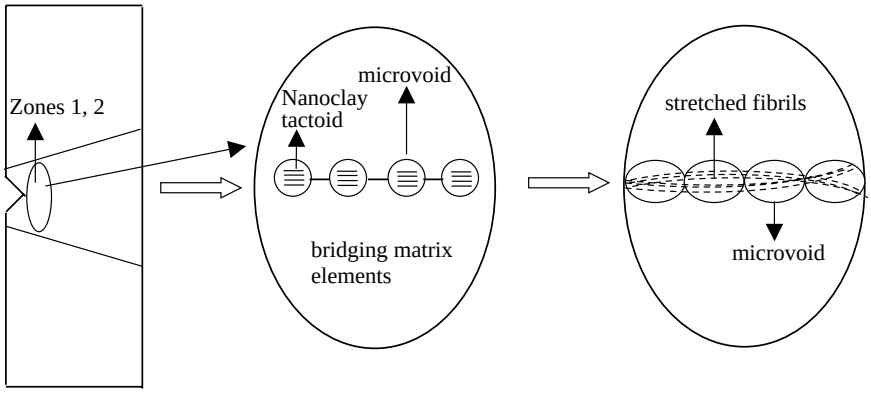

Fig. 10. Schematic of the envisaged microvoid coalescence-fibrillated fracture process operative in PP–clay nanocomposite.

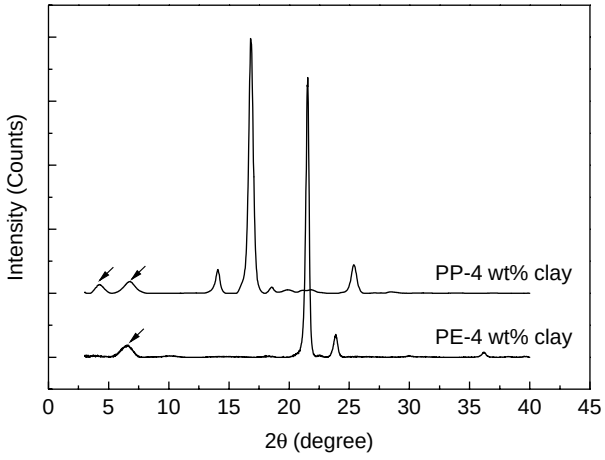

Fig. 11. WAXD patterns of PE-4 wt% clay and PP-4 wt% clay nanocomposites. Arrows point to the (001) peaks of clay.

study on PE–clay system and the present study on PP–clay systems. There are two peaks ($2\theta = 4.2$ and 6.7) corresponding to nanoclay particles in PP–clay nanocomposite, while only one peak ($2\theta = 6.5$) is observed in the clay–reinforced PE nanocomposite for identical clay content (Fig. 11). The presence of lower angle peak in PP–clay nanocomposite suggests larger clay *d*-spacing formed in clay–reinforced PP nanocomposite, which helps in the mobility of PP chains during crystallization. As a consequence, PP in the presence of clay crystallizes at higher temperature than neat PP, while the crystallization temperature only slightly increased in clay–reinforced PE. This argument is further corroborated with the recent results of Xu et al. [48], where they observed that the exfoliated PE–clay sample exhibited higher crystallization temperature than the intercalated PE–clay sample.

Also, in general, for inorganic particle reinforced polymer, the particle–matrix interaction is an important factor in determining the ultimate mechanical properties of composites because a weak interface would impart lower yield strength. PE–clay system [43], which was characterized by higher crystallinity, similar yield strength, weak interfacial interaction between clay and polymer matrix resulted in decrease in toughness. As described in Section 3.1, yield strength of clay–reinforced PP was higher than neat PP and is indicative of strong interaction between nanoclay particles and polymer matrix.

In our case, based on the DSC, PLM, WAXD, TEM and DMA results, we believe that the effect of nucleation and strong interaction between clay and polymer matrix, in conjunction with greater inter-gallery space and improved dispersion state is responsible for the enhancement of toughness of PP–clay nanocomposite.

4. Conclusions

1. The addition of clay to PP increases the impact strength in the temperature range of 0 to +70 °C, while the toughness remained unaffected between −40 to 0 °C.
2. Impact fracture surface of neat PP and clay–reinforced PP nanocomposite exhibits two primary zones: initiation and propagation zones. The fracture initiation and propagation of neat PP is characterized by crazing and vein-type features.
3. The reinforcement of PP with nanoclay alters the primary mechanism of plastic deformation from crazing and vein-type to microvoid-coalescence fibrillation process.
4. The high toughness of clay–reinforced PP nanocomposite is related to the crystal structure and dispersion state of nanoclay particles, and strong interfacial interaction between the nanoclay and polymer matrix.

Acknowledgements

We gratefully acknowledge Ms. Guiyan Zhao for help with the PLM. The authors thank Mr G. Zollos for provision of experimental material.

References

[1] Chapleau N, Mohanraj J, Ajji A, Ward IM. Polymer 2005;46:1956.
[2] Yuan Q, Jiang W, Zhang HX, Yin JH, An LJ, Li RKY. J Polym Sci, Part B: Polym Phys 2001;38:1855.
[3] Liang JZ, Li RKY. Polymer 1999;40:3191.
[4] Yuan Q, Jiang W, An LJ, Li RKY. Polym Adv Technol 2004;15:409.
[5] Liang JZ, Li RKY. Polym Compos 1998;19:698.
[6] Zuiderduin WCJ, Westzaan C, Huétink J, Gaymans RJ. Polymer 2003;44:261.
[7] Hadal RS, Misra RDK. Mater Sci Eng A 2004;374:374.
[8] Hadal RS, Misra RDK. Mater Sci Eng A 2004;380:326.
[9] Trotigon JP, Verdu J, de Vallios A. In: Sedlaucek B, editor. Polymer composites: proceedings of prague IUPAC microsymposium on macromolecules, July 8-11. New York: De Grugter; 1985. p. 191.
[10] Dasari A, Sarang S, Misra RDK. Mater Sci Eng A 2004;368:191.
[11] Dasari A, Rohrmann J, Misra RDK. Mater Sci Eng A 2004;364:357.
[12] Dasari A, Misra RDK. Acta Materialia 2004;52:1683.
[13] Chan CM, Wu J, Li JX, Cheung YK. Polymer 2002;43:2981.
[14] Thio YS, Argon AS, Cohen RE, Weinberg M. Polymer 2002;43:3661.
[15] Haworth B, Raymond CL, Sutherland I. Polym Eng Sci 2001;41:1345.
[16] Albano C, Gonzalez J, Ichazo M, Rosales C, de Navarro CU, Parra C. Compos Struct 2000;49:48.
[17] Wang Y, Wang JJ. Polym Eng Sci 1999;39:190.
[18] Gonzalez J, Albano C, Ichazo M, Diaz B. Eur Polym J 2002;38:2465.
[19] Price GJ, Ansari DM. Polym Int 2004;53:430.
[20] Vollenberg PHT, Heikens D. J Mater Sci 1990;25:3089.
[21] Misra RDK, Nerlikar P, Bertrand K, Murphy D. Mater Sci Eng A 2004;384:284.
[22] Tanniru M, Misra RDK, Bertrand K, Murphy D. Mater Sci Eng A 2005;404:208.
[23] Tanniru M, Misra RDK. Mater Sci Eng A 2005;405:178.
[24] Nathani H, Dasari A, Misra RDK. Acta Materialia 2004;52:3217.
[25] Giannelis EP, Krishnamoorti R, Manias E. Adv Polym Sci 1999;138:107.
[26] Hadal R, Yuan Q, Jog JP, Misra RDK. Mater Sci Eng A 2006;418:268.
[27] Moussaif N, Groeninckx G. Polymer 2003;44:7899.
[28] Alexandre M, Dubois P. Mater Sci Eng 2000;28:1.
[29] Giannelis EP. Flame retardant nanocomposites materials. NIST Annual Conference on Fire Research, Gaithersburg, MD; 1998.
[30] Ozin GP. Adv Mater 1992;4:612.
[31] Alivisatos P, Barbara PF, Castleman AW, Chang J, Dixon DA, Klein ML, et al. Adv Mater 1998;10:1297.
[32] Mann S. Nature 1993;365:499.

[33] Shah D, Maiti P, Gunn E, Schmidtt DF, Jiang DD, Batt CA, et al. Adv Mater 2004;16:1173.
[34] Giannelis EP. Toughnening of a brittle glassy polymer, poly(lactide-*co*-glycolide) by layered silicate nanoparticles. Private Communication; 2005.
[35] Gianelli W, Ferrara G, Camino G, Pellegatti G, Rosenthal J, Trombini RC. Polymer 2005;46:7037.
[36] Thridandapani RR, Mudaliar A, Yuan Q, Misra RDK. Mater Sci Eng A 2006;418:292.
[37] Misra RDK, Nathani H, Dasari A, Wanjale SD, Jog JP. Mater Sci Eng A 2004;386:175.
[38] Wunderlich B. Macromolecular physics. Crystal melting, vol. 3. New York: Academic press; 1980.
[39] Bassett DC. Principles of polymer morphology. UK: Cambridge University Press; 1981.
[40] Jog JP. Mater Sci Technol; in press.
[41] Seki M, Thurman DW, Oberhauser JP, Kornfield JA. Macromolecules 2002;35:2583.
[42] Elmoumni A, Winter H, Waddon AJ, Fruitwala H. Macromolecules 2003; 36:6453.
[43] Tanniru M, Yuan Q, Misra RDK. Polymer 2006;47:2133.
[44] Brown N, Ward IM. J Mater Sci 1983;18:1405.
[45] Misra RDK, Hadal R, Duncan SJ. Acta Mater 2004;52:4363.
[46] Raw S, Takahashi K. Polym Eng Sci 2002;42:2146.
[47] Li ZM, Qian ZQ, Yang MB, Yang W, Xie BH, Huang R. Polymer 2005; 46:10466.
[48] Xu JT, Wang Q, Fan ZQ. Eur Polym J 2005;41:3011.
[49] Hominga DS, Goderis B, Mathot VBF, Groeninckx G. Polymer 2006;47:1630.